

Contribution to the benchmark for ternary mixtures: Transient analysis in microgravity conditions*

Amirhossein Ahadi^a and M. Ziad Saghir

Microgravity Laboratory, Mechanical and Industrial Engineering Department, Ryerson University, Toronto, M5B 2K3, Canada

Received 16 July 2014 and Received in final form 22 August 2014

Published online: 27 April 2015 – © EDP Sciences / Società Italiana di Fisica / Springer-Verlag 2015

Abstract. We present a transient experimental analysis of the DCMIX₁ project conducted onboard the International Space Station for a ternary tetrahydronaphthalene, isobutylbenzene, *n*-dodecane mixture. Raw images taken in microgravity environment using the SODI (Selectable Optical Diagnostic) apparatus which is equipped with two wavelength diagnostic were processed and the results were analyzed in this work. We measured the concentration profile of the mixture containing 80% THN, 10% IBB and 10% *n*C₁₂ during the entire experiment using an advanced image processing technique and accordingly we determined the Soret coefficients using an advanced curve-fitting and post-processing technique. It must be noted that the experiment has been repeated five times to ensure the repeatability of the experiment.

Nomenclature

Change in refractive index	Δn
Maximum concentration difference	ΔC
Maximum temperature difference (K)	ΔT
Coordinate index of pixel	i, j
Initial concentration of i -th component	$C_{0,i}$
Temperature (K)	T
Optical path of the cell (mm)	L
Phase distribution	$\Delta\varphi$
Thermal contrast factor (K ⁻¹)	$\left(\frac{\partial n}{\partial T}\right)$
Concentration contrast factor	$\left(\frac{\partial n}{\partial C}\right)$
Time (s, min, h)	t
Temperature at the hot side of the cavity (K)	T_h
Temperature at the cold side of the cavity (K)	T_c
Molecular diffusion coefficient (m ² s ⁻¹)	D
Thermodiffusion coefficient (m ² s ⁻¹ K ⁻¹)	D'_T
Soret coefficient (K ⁻¹)	S'_T
Concentration at the cold wall (mass fraction)	C_c
Concentration at the hot wall (mass fraction)	C_h
Laser wavelength (nm)	λ
Cartesian co-ordinates in a 2D plane	x, y

Subscript

Minute	min
Reference	ref
Thermal	th
Steady	st

1 Introduction

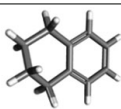
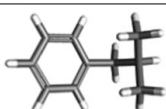

The Soret effect is a phenomenon causing mass transfer in a liquid or gas mixture due to a local temperature gradient [1–4]. This phenomenon should be accurately modeled and considered since it is more pronounced in a porous environment [5, 6]. The Soret effect has applications in environment discovery [7], microfluidic applications [8, 9], particle motion in microfluidic devices [10], and in the field of DNA studies [11, 12], while one of the most important roles of this phenomenon can be seen in the mass transfer in oil reservoirs [13] in which there exists a thermal gradient along the reservoirs. Further analysis indicated that thermodiffusion played the main role in displacing the fluid and moving the gas below the fluid surface [13–15]. Therefore, accurate measurements of thermodiffusion, diffusion and Soret coefficients are vital important in oil exploration and optimal oil recovery. Hence, a precise and better understanding of thermodiffusion phenomena in multi-component mixtures would result in a more accurate modeling of oil reservoirs [16, 17].

Accordingly, there are many teams all around the world currently studying Soret effect for binary, ternary and multi-component mixtures. Measurement of the Soret coefficient faces some technical difficulties in ground conditions because of Earth gravity which causes convective instabilities in the cavity domain [18, 19]. Soret experiments conducted in a microgravity environment can minimize the perturbation effects of gravity, while the impact of g -jitter vibration must be considered [1, 3, 16, 17]. Thus, some of the international thermodiffusion teams are analyzing the results coming from the International Space Station (ISS). In the framework of a cooperative

* Contribution to the Topical Issue “Thermal non-equilibrium phenomena in multi-component fluids” edited by Fabrizio Crocco and Henri Bataller.

^a e-mail: aahadi@ryerson.ca

Table 1. Molecular properties of three components of the test mixture [16].

Molecular structure	THN, C ₁₀ H ₁₂	IBB, C ₁₀ H ₁₄	<i>n</i> C ₁₂ , C ₁₂ H ₂₆
			
Molecular mass	132.21 (g mol ⁻¹)	134.22 (g mol ⁻¹)	170.34 (g mol ⁻¹)

international DCMIX project to measure the Soret and diffusion coefficients of mixtures (DCMIX), all international teams have agreed to present the results of their measurement for THN-IBB-*n*C₁₂ (80:10:10) mixture.

The SODI-DCMIX (Selectable Optical Diagnostic-Diffusion Coefficients of MIXture) project is supported by ESA, and it gathered Canadian, European and Russian scientists to obtain reliable benchmark measurement on ground and onboard ISS [20–23]. The raw images taken in microgravity environment using the SODI apparatus which is equipped with two wavelength diagnostics are processed and the results are analyzed in this work. We measured the concentration profile over the time for all three components using an advanced image processing technique and accordingly we determined the Soret coefficients using an advanced curve-fitting and image processing technique. It must be noted that the experiment has been repeated few times to ensure the repeatability of the space experiment and the results are reported here. In the next two sections, the SODI-DCMIX₁ projects and the mass fluxes in a ternary system in the presence of a temperature gradient are mathematically described. Section 4 briefly explains the mathematical approach used for image processing and extracting information from the raw data. Results and discussion are provided in sect. 5. Finally, the summary and conclusions are drawn in sect. 6.

2 DCMIX onboard the International Space Station

The SODI (Selectable Optical Diagnostic) apparatus, was launched to the International Space Station in 2009. It is located inside the Microgravity Science Glovebox. The Glovebox is one of the major dedicated science facilities inside the Destiny lab. As shown in fig. 1, it has a large front window and built-in gloves to allow a sealed environment to perform experiment with different exchangeable optical techniques. SODI apparatus includes an optical interferometer, it allows sending the real time images taken during the experiment to researchers via telemetry [17, 18, 24].

2.1 Benchmark mixture

The most usual ternary mixture used by oil industry for their modeling is composed of 1,2,3,4-tetrahydronaph-



Fig. 1. ESA Image, Microgravity Science Glovebox (MSG), see ref. [25].

thalene (THN), isobutylbenzene (IBB) and *n*-dodecane (*n*C₁₂) representing different molecule families (polycyclic, alkane, aromatic) [16], see table 1 for more detail.

Consequently, this mixture can be used as a benchmark mixture for various measurement in the field of oil industry analysis. The instrument SODI is equipped with two wavelength diagnostic (MR: $\lambda = 670$ nm and MN: $\lambda = 935$ nm) which enables the measurement of the Soret and diffusion coefficients in ternary mixtures. According to the international agreement between all teams, it was decided to perform the benchmark analysis for the fluidic cell that contains 80% THN, 10% IBB and 10% *n*C₁₂.

2.2 Experimental apparatus

The apparatus on board the ISS is equipped with a Mach-Zehnder interferometer, particle image velocimeter, and near field scattering measurement equipment [18, 21]. While most parts of the apparatus are fixed for each particular experiment, the cell array of experimental cells can be changed from one experiment to another.

The mixture was contained in a 10 mm × 10 mm × 5 mm (width, length, height) cell and monitored by a Mach-Zehnder interferometry (MZI) apparatus using two laser beams with different wavelengths (670 nm MR laser and

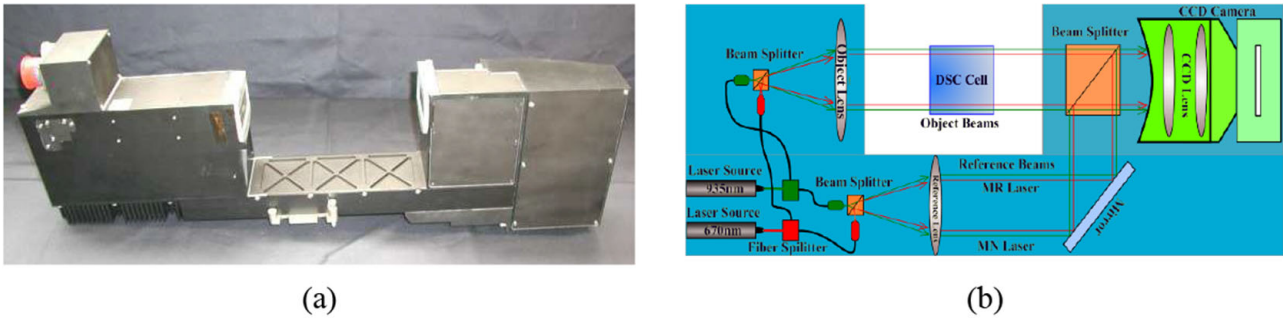


Fig. 2. Digital interferometry instrument moving bridge onboard ISS and its scheme [16].

935 nm MN laser). Figure 2a) and b) shows an image of the actual optical digital interferometry instrument apparatus and its schematic setup, respectively. More information about the optics contained in various modules is given in the optical design report [16].

2.3 Experimental principle and procedure

The beam which was created by any of the laser sources was expanded by a spatial filter and then passed through a beam splitter. One of the beams then passed through the cell and the other beam bypassed the cell and was used as reference beam. Figure 2 demonstrates the two different paths inside the cell holder. After passing the mirrors, the two beams interfered with each other at a second beam splitter.

The sequences of the experiment are as follows: 1) Thermalization of the sample at the mean temperature of 25 °C so that a uniform concentration and temperature inside the cavity would be obtained. 2) Application of thermal gradient over 6 to 8 hours depending use of the Peltier elements' and thermal controller unit [16]. Consequently, the temperature field achieved thermal stability within few minutes. 3) The temperature gradient was removed, which resulted in returning to the initial condition. MZI images and the Peltier elements' temperature were recorded and sent to the scientists during all steps of the experiment. The entire procedure has been repeated few times to assure the repeatability of the results [16].

3 Soret mass fluxes in ternary mixtures

Due to the Soret effect in a mixture with n components, there are n mass fluxes. Each mass flux has n terms, $n - 1$ terms reflect the mass fluxes due to molecular diffusion and the last term represents the mass flux due to the thermodiffusion in a mixture with n components. Note that all fluxes have opposite direction to the temperature gradient [16, 23]. Accordingly, the mass flux of any ternary mixture can be represented using the three sources of mass

flux as follows [16]:

$$\vec{J}_1 = -\rho D_{11} \left(\nabla c_1 + \frac{D_{12}}{D_{11}} \nabla c_2 + S_{T1} \nabla T \right), \quad (1)$$

$$\vec{J}_2 = -\rho D_{22} \left(\frac{D_{21}}{D_{22}} \nabla c_1 + \nabla c_2 + S_{T2} \nabla T \right), \quad (2)$$

$$\sum_{i=1}^3 \vec{J}_i = 0, \quad (3)$$

where the Soret coefficient of the i -th component is $S'_{T,i} = \frac{D'_{T,i}}{D_{ii}}$, ρ is the density of the mixture, c_i is the mass fraction of the i -th component, D_{ij} is the pure diffusion coefficients when $i = j$ and is the cross-diffusion coefficients when $i \neq j$; finally, $D'_{T,i}$ represents the thermodiffusion coefficients of the i -th components in the ternary mixture.

4 Image processing method

4.1 Phase extraction

While DCMIX aimed to employ the phase shift technique for MZI [17, 23], it was observed that, because of the close response of the light sources, Fourier transform image processing method may provide a better result [26, 27]. It should be noted that another member of the thermodiffusion international team is processing the results of DCMIX using the phase shifting method, which would be published separately. After downloading the raw images and converting them to bitmap images, all interferograms were subjected to an identical cropping. We believe that cropping the specific region of the cell is essential in order to obtain an accurate result because of the following reasons: 1) to remove crashed pixels around the walls which may be caused by the reflection of the light from the walls, 2) to remove the areas close to the hot and the cold walls that experienced higher temperature gradient and 3) to remove the lateral regions with heat losses from the lateral walls. Higher temperature gradient close to the cold and the hot walls and also heat fluxes toward the lateral walls can be observed when the entire temperature contour was

Table 2. Compositions and optical properties of the benchmark ternary mixture cell #3 [32].

Initial mass fraction			MR Laser $\lambda = 670$ nm		MN Laser $\lambda = 935$ nm	
THN	IBB	nC_{12}	$\left. \frac{\partial n}{\partial c_{\text{THN}}} \right _{\text{IBB}, T, p}$	$\left. \frac{\partial n}{\partial c_{\text{IBB}}} \right _{\text{THN}, T, p}$	$\left. \frac{\partial n}{\partial c_{\text{THN}}} \right _{\text{IBB}, T, p}$	$\left. \frac{\partial n}{\partial c_{\text{IBB}}} \right _{\text{THN}, T, p}$
80%	10%	10%	0.14277	0.08869	0.13736	0.08376

measured during the experiment. The next step in the image processing is the phase extraction from fringe domain. For a ternary system, four images must be taken simultaneously in each loop of image processing. Two reference images that remained constant throughout the experiment were employed to normalize the MN and MR images. In the next step, the phase map which varies from $-\pi$ to $+\pi$ must go through the unwrapping procedure [28–30]. Thus, $\Delta\phi$, or phase distribution, can be determined by the difference between the phase of the i -th image and the reference image [31]

$$\Delta\phi(x, y, t_i) = \phi(x, y, t_i) - \phi_{\text{ref}}(x, y). \quad (4)$$

4.2 Refractive index measurement

The phase difference obtained by the unwrapping process was used to calculate $\Delta n(x, y)$. Knowledge of the refractive index distribution allowed the calculation of the temperature and concentration variations in the cell, and, consequently, the maximum temperature and concentration differences. The refractive index variation (Δn) can be obtained from the phase difference $\Delta\phi$ as presented as follows:

$$\Delta n(x, y) = n(x, y) - n_{\text{ref}}(x, y) = \frac{\lambda}{2\pi L} \Delta\phi(x, y), \quad (5)$$

where L is the thickness of the liquid layer that the laser light passed through and λ is the wavelength of the laser. Since there are two lasers implemented in the SODI apparatus to analyze ternary mixtures, all of the processing and the equations should be applied for both lasers separately.

4.3 Concentration measurement

The changes of the refractive index in the domain result from changes in temperature and concentration in the domain as follows:

$$\begin{aligned} \Delta n_1(x, y) &= \left(\frac{\partial n_1}{\partial T} \right)_{T_0, C_0, \lambda_1} \Delta T(x, y) \\ &+ \left(\frac{\partial n_1}{\partial c_1} \right)_{T_0, C_2, \lambda_1} \Delta C_1(x, y) \\ &+ \left(\frac{\partial n_1}{\partial c_2} \right)_{T_0, C_1, \lambda_1} \Delta C_2(x, y), \end{aligned} \quad (6)$$

$$\begin{aligned} \Delta n_2(x, y) &= \left(\frac{\partial n_2}{\partial T} \right)_{T_0, C_0, \lambda_2} \Delta T(x, y) \\ &+ \left(\frac{\partial n_2}{\partial c_1} \right)_{T_0, C_2, \lambda_2} \Delta C_1(x, y) \\ &+ \left(\frac{\partial n_2}{\partial c_2} \right)_{T_0, C_1, \lambda_2} \Delta C_2(x, y), \end{aligned} \quad (7)$$

where, $\Delta T(x, y)$ and $\Delta C(x, y)$ represent the maximum temperature and concentration changes at the point (x, y) , respectively, $(\partial n/\partial T)$ is the variation of the refractive index due to temperature, and $(\partial n/\partial c)$ is the variation of the refractive index due to concentration. After thermal time, the derivative of temperature with respect to time is equal to zero and eqs. (6) and (7) were combined as follows:

$$\begin{aligned} \begin{bmatrix} \Delta C_i(x, y) \\ \Delta C_j(x, y) \end{bmatrix} &= \\ \begin{bmatrix} \left. \frac{\partial n_i}{\partial c_i} \right|_{T_0, C_j, \lambda_1} & \left. \frac{\partial n_i}{\partial c_j} \right|_{T_0, C_i, \lambda_1} \\ \left. \frac{\partial n_j}{\partial c_i} \right|_{T_0, C_j, \lambda_2} & \left. \frac{\partial n_j}{\partial c_j} \right|_{T_0, C_i, \lambda_2} \end{bmatrix}^{-1} & \begin{bmatrix} \Delta n_1(x, y) \\ \Delta n_2(x, y) \end{bmatrix}. \end{aligned} \quad (8)$$

The concentration contrast factors for wavelengths $\lambda = 670$ nm and $\lambda = 935$ nm were obtained from the literature [32] at the relevant compositions for the benchmark composition of this ternary mixture and these coefficients are shown in table 2. It should be noted that the thermal time here is estimated based on a recent study [33] that considers the effect of the separation of the components during the thermal time.

4.4 Post-processing of the result to estimate Soret and diffusion coefficients

In the steady-state regime upon reaching the diffusion time, the Soret coefficients for the i -th components were calculated in the literature as follows [16, 34–36]:

$$S_{T_i} = -\frac{\Delta C_{i, \text{st}}}{C_0(1 - C_0)\Delta T}, \quad (9)$$

where $\Delta C_{i, \text{st}}$ is the stationary separation of component i , $C_{i,0}$ is the initial mass fraction of component i , and S_{T_i} represents the Soret coefficient of the i -th component. This definition of the Soret effect is widely used for binary

mixtures; however, our analysis based on the results of the DCMIX project showed that using the same equation to define the Soret coefficient for ternary mixtures does not present the tendency of the components of the mixture to separate toward the cold or the hot walls. This is because of the pre-factor $C_0(1-C_0)$ in the denominator. This term in the dominator has a stronger impact on the value of the Soret effect than ΔC in the nominator. Consequently, S_T would be a strong function of the initial composition of the mixture and not the maximum separation due to Soret effect. Because of this reason, the international thermodiffusion team has agreed to use the modified formula to calculate the Soret coefficients for ternary mixtures in which the pre-factor has been removed as follows;

$$S'_{Ti} = -\frac{\Delta C_{i,st}}{\Delta T} \quad (10)$$

Note that this equation can be used when the steady-state condition for the separation of the components is reached; while the time scheduled for the separation of the components was not sufficient to reach the steady-state condition, the aided GA with fast robust discretized smoothing can be implemented to find the curve that provides the best fit to the experimental separation [16]. For this case, the analytical or numerical transient profile of the separation must be used as the fitting curve. This profile is a function of the Soret and the diffusion coefficients of the components. Thus, the fitting procedure determines the best analytical (or numerical) fit to the experimental results to estimate the S'_T and D simultaneously using an EA (Evolutionary Algorithm). The application of GA (Genetic Algorithm) for the nonlinear problem has been approved [37], so this method can precisely estimate the Soret and diffusion coefficients concurrently when a proper objective function is chosen [16,23].

5 Results and discussions

The SODI-DCMIX cell array onboard the ISS has six cells. Five of these cells contained ternary mixtures at various compositions. Here, we analyzed the results of the third cell that contained 80% THN, 10% IBB and 10% nC_{12} . The refractive index and concentration contours were measured inside the cell using MZI. The goal of this study is to measure the Soret coefficients of this ternary mixture, while the diffusion coefficient of the mixture can be measured using the same technique simultaneously. It is worth noting that comprehensive studies on the quality of the SODI-DCMIX apparatus have been done previously [16,17,20].

The first optical parameter that would be obtained from the image processing is the refractive index variation during the experiment. Figure 3 shows the refractive index difference between the hot and cold walls for Run3 with $\Delta T = 10$ K (according to the DCMIX₁ time table) in which 94 percent of the height of cell 3 has been processed. The refractive index measured using both lasers showed similar behavior, however, the value of Δn measured by

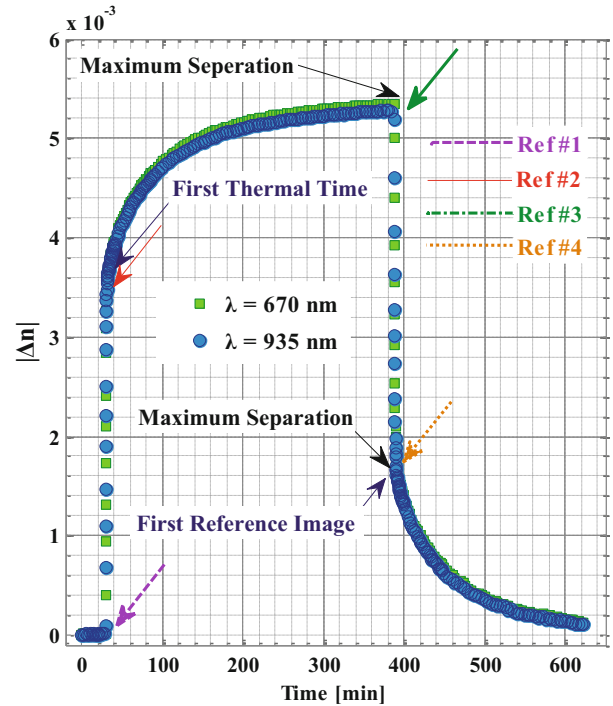


Fig. 3. Absolute refractive index difference between the hot and cold walls for Run 33, in which 94 percent of the height of the cell is considered.

the 670 nm laser always gave a higher value. Considering this small difference in the behaviors of the lasers along with the slight variation of contrast factors between these two lasers, the separations in the ternary system for all three components were extracted. This can be observed in fig. 3, in which the data points with maximum separation are pointed out with black arrows. For the post-processing of the results, four reference images must be considered as shown in fig. 3. The first reference represents the initial condition ($T = 25^\circ\text{C}$ and $\Delta C_i = 0$), Reference 2 should be considered in one thermal time after application of the thermal gradient. However, in order to consider the separation during the first thermal time, the second reference image can be considered few seconds before the thermal time [33], (as shown by the red arrow in fig. 3).

References 3 and 4, that are illustrated with the green and orange arrows, must be considered to measure the temperature variation after removing the temperature gradient and until one thermal time. Reference 4 must also be employed to measure the concentration profiles during the diffusion time (last 3 hours of the experiment). Finally, it should be noted that the smooth patterns of the refractive indices could be seen. This shows the small uncertainty in this experiment; however, because of a similar response of both lasers, the accuracy of the post-processing of the experiment and the measurement of the concentration profiles highly depends on the uncertainties of the contrast factors.

A linear variation of the temperature along the height of the cell is an essential condition to have pure thermodiffusion separation in the mixture. This condition can be

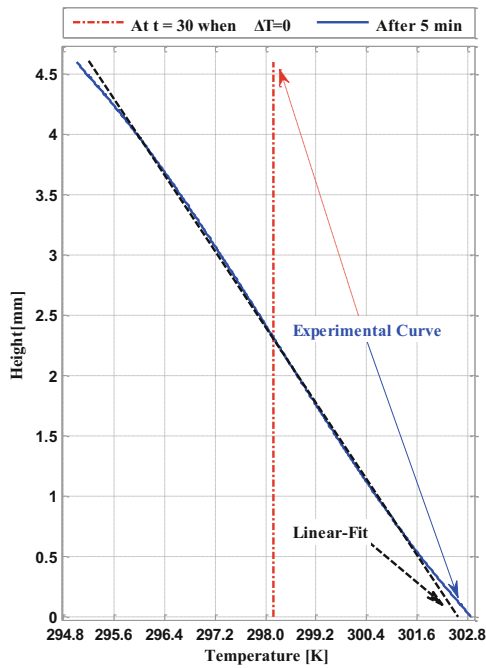


Fig. 4. Temperature variation between hot and cold walls in the presence of the temperature gradient and at the beginning of the experiment for Run 33.

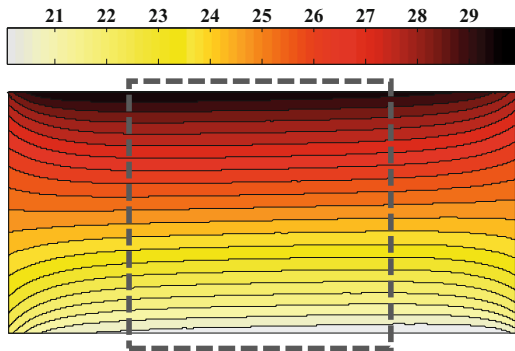


Fig. 5. Temperature contour after 5 minutes of applying temperature difference with the assigned $\Delta T = 10$ K for Run 33.

confirmed for the central region of cell 3 [16]. Figure 4 shows the temperature variation along the height of the cell measured at the beginning of the experiment when there was no temperature difference and after 5 minutes of application of thermal gradient. While at the beginning, a linear temperature curve has been obtained (red dashed line), this observation after one thermal time is true for the central region (blue solid line). It is evident that as much as the location is closer to the hot or cold walls, the deviation from the linear variation is stronger. This is the main reason for removing the region close to the walls [20,24,38]. The Linear-Fit line in fig. 4 shows the deviation from linear temperature variation after 5 minutes. Accordingly, 89 to 94 percent of the height of the cell at the center was considered to analyze the Soret effect in the ternary mixture in this study.

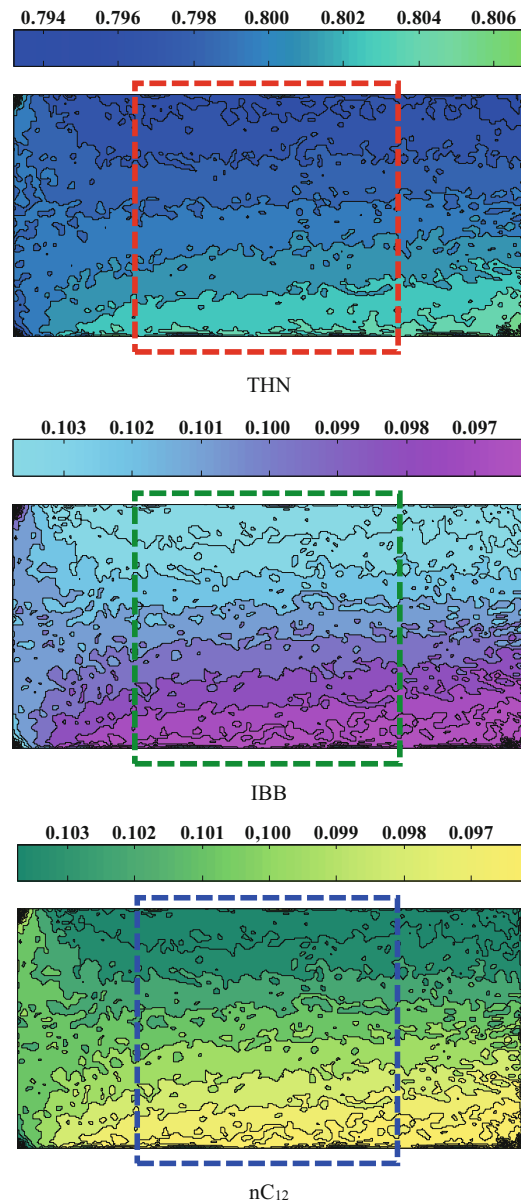


Fig. 6. Concentration contours of THN, IBB and nC_{12} after 6 hours of thermodiffusion process with the assigned $\Delta T = 10$ K for Run 33.

On the other hand, the region close to the lateral walls must be removed from the post-processing of the image processing results. The curvature of the temperature profile close to the corners of the cell is evident in fig. 5. This is because of the heat losses at the lateral walls [19,24]. Consequently, only 50 percent of the length of the cell (~ 5 mm) in the middle region of the cell was considered in this study. The region is indicated by the dashed lines in fig. 5. The concentration contours for all three components of the mixture have been measured using eq. (8) for Run 33 after 6 hours of application of the thermal gradient. The results are shown in fig. 6; while the temperature contour shows some smooth profiles, it can be seen that the calculated concentration profiles show a wiggly pattern.

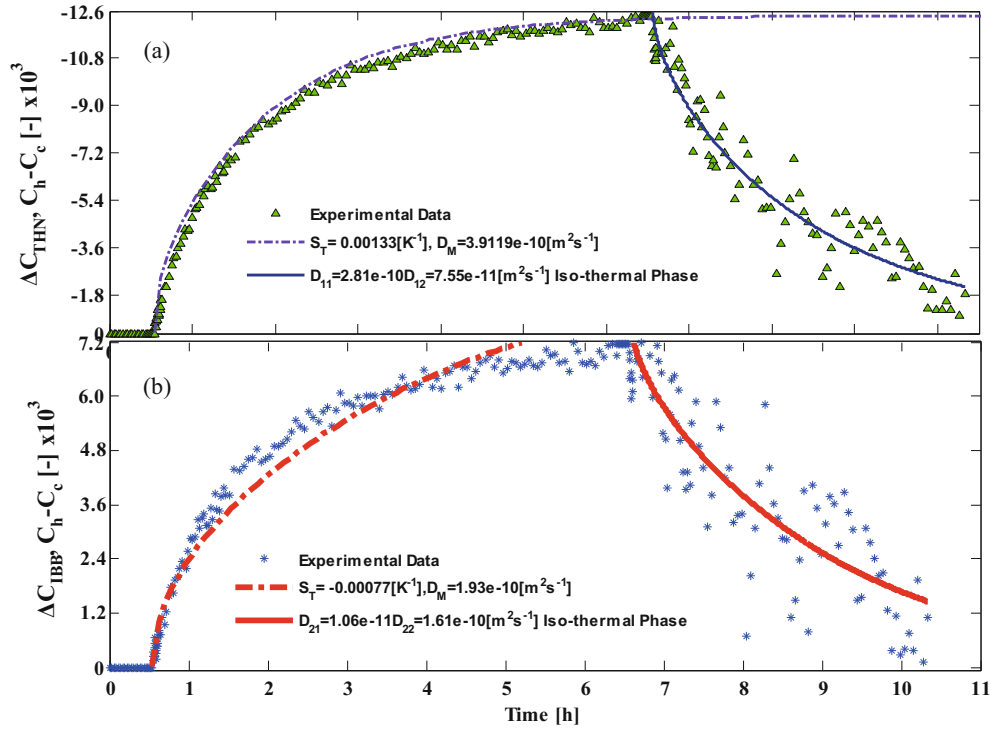


Fig. 7. Concentration difference between the hot and cold sides *versus* time during thermodiffusion and diffusion phases for Run 3.

Table 3. Detailed experimental results of the thermodiffusion experiments of the ternary mixture inside cell #3 on board the ISS.

Run #	Cropped height (mm)	ΔT (°C)	Maximum refractive index difference $\Delta n \times 10^4$				Maximum Concentration Difference $\times 10^3$ (-)		
			Thermal time		Thermodiffusion time		THN	IBB	nC_{12}
			$\lambda_1 = 670$ nm	$\lambda_2 = 935$ nm	$\lambda_1 = 670$ nm	$\lambda_2 = 935$ nm			
3	4.68	9.35	39.7	39.3	10.99	10.69	-11.67	6.38	5.29
13	4.44	8.88	37.5	36.9	9.15	8.90	-10.43	6.47	3.96
18	4.65	9.31	3.95	39.1	10.63	10.34	-11.89	7.15	4.74
28	4.69	9.38	40.1	39.9	10.90	10.59	-11.69	6.52	5.16
33	4.69	9.37	40.6	40.1	10.82	10.53	-12.30	7.60	4.70

As mentioned before, because of the heat flux at the boundaries, a linear diffusion pattern cannot be observed at the boundaries. In particular, the separations close to lateral walls were smaller than the separation at the central region. It can be observed that there is no noticeable separation close to the left walls, this means that the heat flux from one of the lateral walls had a stronger impact on diminishing the Soret effect. Eventually, it should be noted that, to study the Soret effect, the regions inside the dashed lines are considered. As it is evident in this figure, the separation of THN is two times stronger than IBB and nC_{12} and it is separated toward the cold region of the cell. On the other hand, both IBB and nC_{12} have moved toward the hot walls with similar magnitude. Finally, the linear variation of the concentrations from the hot wall toward the cold wall points out the pure thermodiffusion procedure occurring inside the four dashed lines.

The maximum concentration difference of THN and IBB for cell 3 with $\Delta T = 10$ K for Run 3 is plotted in fig. 7a) and b), respectively. Separating toward the cold side of the cell for THN means a positive Soret effect. The THN and IBB separations for Run 13 (same conditions as Run 3) are also plotted in fig. 7, to compare the transient separation for two similar runs. It can be seen in this figure that both runs have provided quite similar results; however, the separations for Run 3 is slightly greater than Run 13 and this is because the cropping size with respect to the height of the cell for Run 3 was greater. See table 3 for more detail on the cropping size of each run.

It can be seen in fig. 7 and fig. 8 that the pure diffusion coefficient of THN is greater than IBB, because THN showed the faster separation during first 6 hours. Eventually, the experimental results during the thermodiffusion phase provide smooth behaviors, while the experimental uncertainty for the diffusion phase was greater. Another

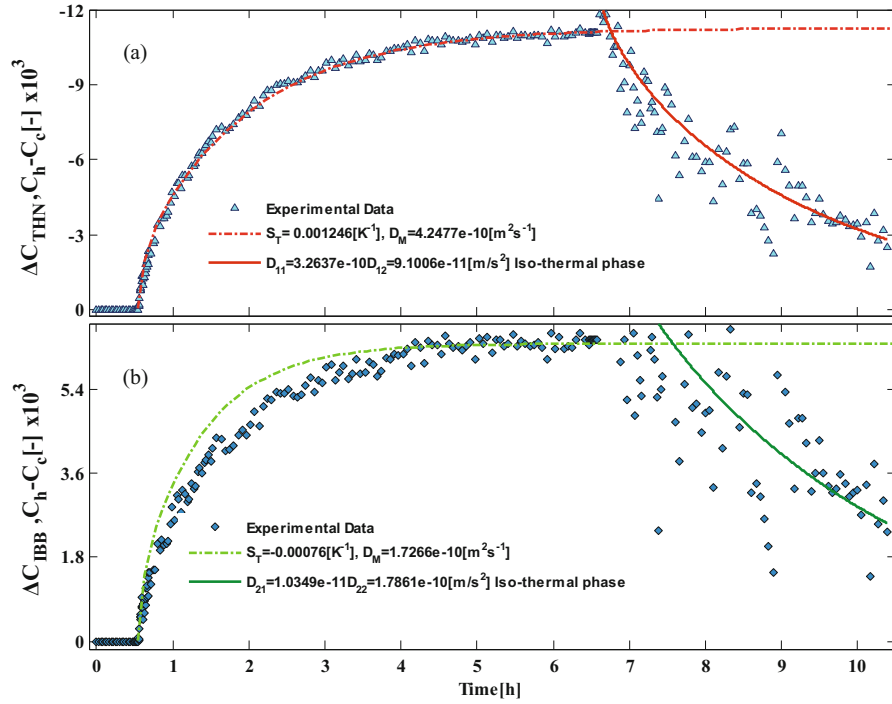


Fig. 8. Concentration difference between the hot and cold sides *versus* time during thermodiffusion and diffusion phases for Run 13.

Table 4. Soret coefficients of the ternary mixture measured in microgravity environment for five runs.

Run #	$S'_{T,THN} \times 10^3$	$S'_{T,IBB} \times 10^3$	$S'_{T,nC12} \times 10^3$
3	1.334	-0.770	-0.621
13	1.244	-0.764	-0.490
18	1.406	-0.845	-0.560
28	1.371	-0.765	-0.605
33	1.443	-0.892	-0.551
Average	1.369	-0.815	-0.566
Standard deviation	0.059	0.054	0.052

fact that is concluded from these figures is that the steady-state separation is not reached after 6 hours of thermodiffusion since the slope of the separation is evident during the last hour of the thermodiffusion phase.

Accordingly, the curve fitting with four free parameters during the thermodiffusion phase (two Soret coefficients and two diffusion coefficients) and also four free parameters during the diffusion phase (two Soret coefficients and two diffusion coefficients) must be used to calculate S_T and D . The results of the curve-fitting procedure are also plotted in fig. 7 and fig. 8. Comparing these results with temporal experimental data showed a good match with experimental trends, especially for THN which showed a higher tendency to separate at the presence of thermal gradient.

As stated, the concentration measurement for ternary mixtures using MZI is highly sensitive to the measurement of the concentration contrast factors [16,39]. For ternary

mixture, only few percent inaccuracy in the measurement of the concentration contrast factors may drastically affect the final results. Consequently, in this study, in addition to reporting the maximum temperature and concentration variations and Soret coefficients of the components, we have reported the maximum refractive variation at the end of thermal time and at the end of the thermodiffusion time. These four values, along with the contrast factors, can be yielded in the calculation of the maximum concentration and temperature difference between the cold and hot walls.

In this study, the contrast factors measured by Secheny *et al.* [32] were used. It should be noted that the experiment was repeated more than five times at each specific condition to ensure the repeatability of the experimental results. Here, we reported the results of five runs with identical condition. The four mentioned parameters (Δn) are listed in table 3 for all repeated runs (Run 3, 13, 18,

28 and 33). The height of the cell which is used in the processing of the Soret effect is also reported in table 3. The results of runs are within a reasonable range to consider the experimental results reliable with the maximum standard deviation of 0.059.

It can be seen that for all runs that nC_{12} , with a slight difference from IBB, showed the minimum tendency to separate due to ΔT , while THN showed the maximum. Thus, it can be concluded that the lighter component moved toward the cold side. The molecular masses of THN and IBB are similar; however, the heavier IBB experienced a separation towards the hot side, and THN, which has an intermediate molecular mass, separated toward the cold wall. Taking the results of curve-fitting method and table 3, the Soret coefficients of the components for all repeated runs and their average and standard deviation values can be calculated. All estimated values are reported in table 4. In conclusion, the Soret coefficients of the mixture are $1.369 \pm 0.059 \text{ K}^{-1}$ for THN, $-0.8159 \pm 0.054 \text{ K}^{-1}$ for IBB and $-0.566 \pm 0.052 \text{ K}^{-1}$ for nC_{12} , according to the space experiment results (SODI-DCMIX₁).

6 Conclusion

In the framework of benchmark measurement of the Soret coefficient of a specific ternary hydrocarbon mixture, the space experiment result of the DCMIX₁ project has been analyzed for five repeated runs. The windowed Fourier transform image processing aided by a curve-fitting method and GA was employed to estimate S_T^* . Consequently, the Soret coefficients of 80% THN, 10% IBB, 10% nC_{12} mixture at a mean temperature of 25 °C have been determined. The quite similar results of the repeated runs proved the quality and repeatability of the experiment. The linearity in the temperature variation along the height of the cells was investigated which resulted in removing the regions close to the hot and the cold walls. It was observed that for this specific composition of the mixture, six hours of thermodiffusion time is not sufficient to reach a steady-state separation. This proved the essential application of the curve fitting to measure the Soret coefficients instead of using the steady-state Soret formula. THN which filled the 80% of the cell showed the maximum tendency to separate due to the temperature difference. On the other hand, the separations of IBB and nC_{12} were similar, while the IBB experienced a stronger separation due to Soret effect. It was observed that IBB and nC_{12} moved towards the hot side, and THN with an intermediate molecular mass separated towards the cold wall. Eventually, the Soret coefficients of the mixture were reported for all five repeated runs along with the average value and the standard deviation.

The authors would like to thank the Canadian Space Agency (CSA) and Natural Sciences and Engineering Research Council of Canada (NSERC) for funding this work. We also acknowledge the support of ESA and ROSCOSMOS for providing us with the experimental raw images and facilitating the experiment onboard ISS.

References

1. A. Ahadi, M.Z. Saghir, *Micrograv. Sci. Technol.* **25**, 127 (2013).
2. A. Mialdun, V. Yasnou, V. Shevtsova, A. Königer, W. Koehler, D. Alonso de Mezquia, M.M. Bou-Ali, A. Koniger, D.A. de Mezquia, *J. Chem. Phys.* **136**, 244512 (2012).
3. A. Ahadi, M.Z. Saghir, *Fluid Dynam. Mater. Proc.* **8**, 397 (2012).
4. S. Hartmann, W. Koehler, K.I. Morozov, *Soft Matter* **8**, 1355 (2012).
5. A. Ahadi, T. Yousefi, M.Z. Saghir, *Can. J. Chem. Engin.* **91**, 1918 (2013).
6. M. Mojtabi, Y. Razi, K. Maliwan, A. Mojtabi, *Numer. Heat Transfer Part A* **46**, 981 (2004).
7. J.R. Petit, J. Jouzel, D. Raynaud, N.I. Barkov, J.-M. Barnola, I. Basile, M. Bender, J. Chappellaz, M. Davis, G. Delaygue, M. Delmotte, V.M. Kotlyakov, M. Legrand, V.Y. Lipenkov, C. Lorius, L. PEPin, C. Ritz, E. Saltzman, M. Stievenard, *Nature* **399**, 429 (1999).
8. R. Piazza, *Soft Matter* **4**, 1740 (2008).
9. R. Piazza, A. Parola, *J. Phys.: Condens. Matter* **20**, 153102 (2008).
10. D. Vigolo, R. Rusconi, H.A. Stone, R. Piazza, *Soft Matter* **6**, 3489 (2010).
11. S. Duhr, D. Braun, *Phys. Rev. Lett.* **97**, 038103 (2006).
12. S. Duhr, D. Braun, *Proc. Natl. Acad. Sci. U.S.A.* **103**, 19678 (2011).
13. K. Ghorayeb, A. Firoozabadi, *SPE J., Reservoir Engin. Res. Inst.* **8**, 114 (2003).
14. K. Ghorayeb, A. Firoozabadi, *Soc. Petroleum Engin. J.* **5**, 158 (2000).
15. K. Ghorayeb, T. Anraku, A. Firoozabadi, *SPE Asia Pacific Conference on Integrated Modelling for Asset Management* (2000) pp. 1–10.
16. A. Ahadi, S. Van Varenbergh, M.Z. Saghir, *J. Chem. Phys.* **138**, 204201 (2013).
17. V. Shevtsova, C. Santos, V. Sechenyh, J.C. Legros, A. Mialdun, *Micrograv. Sci. Technol.* **25**, 275 (2013).
18. A. Ahadi, M.Z. Saghir, *Appl. Thermal Engin.* **60**, 348 (2013).
19. A. Ahadi, A. Kianian, M.Z. Saghir, *Int. J. Thermal Sci.* **75**, 233 (2014).
20. A. Mialdun, C. Minetti, Y. Gaponenko, V. Shevtsova, F. Dubois, *Micrograv. Sci. Technol.* **25**, 83 (2013).
21. M. Lappa, *SODI - [Experiment] Mission Operations Implementation Concept* (2011).
22. M.M. Bou-Ali, A. Ahadi, D.A. de Mezquia, Q. Galand, M. Gebhardt, O. Khlybov, W. Köhler, M. Larrañaga, J.C. Legros, T. Lyubimova, A. Mialdun, I. Ryzhkov, M.Z. Saghir, V. Shevtsova, S. Van Varenbergh, *Contribution to the benchmark for ternary mixtures: determination of Soret coefficients by the thermogravitational and the sliding symmetric tubes techniques*, this issue.
23. A. Ahadi, M.Z. Saghir, *Optics Lasers Engin.* **59**, 72 (2014).
24. A. Ahadi, M.Z. Saghir, *Appl. Thermal Engin.* **62**, 351 (2014).
25. “Microgravity Science Glovebox / Columbus / Human Spaceflight / Our Activities / ESA”, available at: http://www.esa.int/Our_Activities/Human_Spaceflight/Columbus/Microgravity_Science_Glovebox.
26. Q. Kema, *Appl. Optics* **43**, 2695 (2004).

27. A. Ahadi, A. Khoshnevis, M.Z. Saghir, *Optics Laser Technol.* **57**, 304 (2014).
28. Q. Kemaο, *Optics Laser Technol.* **40**, 1091 (2008).
29. Q. Kemaο, W. Gao, H. Wang, *Appl. Optics* **49**, 1075 (2010).
30. R.C. González, R.E. Woods, *Digital Image Processing* (Pearson/Prentice Hall, 2008).
31. A. Ahadi, C. Giraudet, H. Jawad, F. Croccolo, H. Bataller, M.Z. Saghir, *Int. J. Thermal Sci.* **80**, 108 (2014).
32. V.V. Sechenyh, J.-C. Legros, V. Shevtsova, *J. Chem. Thermodyn.* **62**, 64 (2013).
33. A. Ahadi, M.Z. Saghir, to be published in *Can. J. Chem. Engin.*
34. A. Kianian, A. Ahadi, M.Z. Saghir, *Can. J. Chem. Engin.* **91**, 1568 (2013).
35. A. Khoshnevis, A. Ahadi, M.Z. Saghir, *Appl. Thermal Engin.* **68**, 36 (2014).
36. A. Khoshnevis, A. Ahadi, M.Z. Saghir, *Int. J. Thermal Sci.* **75**, 221 (2014).
37. R. Khoshrooz, A.M. Vahid, M. Mirshams, M.R. Homaeinezhad, A. Ahadi, *Appl. Mech. Mater.* **110-116**, 4977 (2012).
38. A. Mialdun, V. Shevtsova, *Micrograv. Sci. Technol.* **21**, 31 (2008).
39. V. Shevtsova, A. Nepomnyashchy, J.C. Legros, *Philos. Mag.* **91**, 3498 (2011).